

Shear heating not a cause of inverted metamorphism

Steven B. Kidder^{1*}, Frédéric Herman^{2,3}, Jason Saleeby¹, Jean-Philippe Avouac¹, Mihai N. Ducea^{4,5}, and Alan Chapman⁴

¹California Institute of Technology, 1200 E. California Boulevard, Pasadena, California 91125, USA

²Faculté des Géosciences et de l'Environnement, Université de Lausanne, Geopolis Bureau 3232, 1015 Lausanne, Switzerland

³Earth Sciences Department, ETH, Sonneggstrasse 5, 8092 Zurich, Switzerland

⁴Department of Geosciences, University of Arizona, 1040 E. 4th Street, Tucson, Arizona 85721, USA

⁵Universitatea Bucuresti, Facultatea de Geologie Geofizica, Str. N. Balcescu Nr 1, Bucharest 010041, Romania

ABSTRACT

An archetypal example of inverted metamorphism purportedly resulting from shear heating is found in the Pelona Schist of southern California (United States). Recent studies demonstrate that the Pelona Schist was subducted and accreted at the onset of Laramide flat subduction under thermal and kinematic conditions not considered in earlier numerical models. To test the shear heating hypothesis under these conditions, we constructed a thermokinematic model of flat subduction initiation involving continuous accretion of the schist. A neighborhood algorithm inversion demonstrates that available metamorphic and thermochronologic constraints in the Sierra Pelona mountains are satisfied only if accretion rates were 0.2–3.6 km/m.y and shear heating was minimal (shear stress 0–19 MPa). Minimal shear heating is also consistent with an inversion of models constrained by thermochronology of the East Fork (of the San Gabriel River) exposure of the schist. Shear heating inhibits the formation of modeled inverted gradients during accretion and should not be considered an important factor in their generation.

INTRODUCTION

The interpretation of inverted metamorphic gradients is a long-standing issue in geodynamics with relevance to lithospheric stress levels and crustal dynamics (e.g., England and Molnar, 1993; Jamieson et al., 1996). Shear heating has long been considered a potential cause of inverted metamorphism beneath thrusts (e.g., Graham and England, 1976; Le Fort, 1975) because it provides a heat source that (1) may generate an instantaneous inverted geotherm (e.g., Graham and England, 1976), and (2) could explain peak temperatures at the tops of inverted gradients that are often higher than expected. A commonly cited (e.g., Cooper and Norris, 2011; Nabelek et al., 2010; Pitra et al., 2010) example of inverted metamorphism ascribed to shear heating is the Pelona Schist in the San Gabriel Mountains of southern California (United States). To model the metamorphism of the Pelona Schist, Graham and England (1976)

and England and Molnar (1993) estimated shear stress (τ) on the overlying subduction thrust to be ~100 MPa, an extremely high and debatable value (e.g., Harrison et al., 1999; Kidder and Ducea, 2006). Peacock (1987) demonstrated that heat conduction from a hot upper plate during early stages of subduction could reduce required τ to ~40 MPa. These models, however, (1) neither incorporate accretion nor reflect the modern consensus (e.g., Grove et al., 2003; Saleeby, 2003) that the schist was accreted during early stages of flat and shallow subduction, and (2) were not tested against thermochronologic data, specifically coupled detrital zircon and Ar/Ar data limiting schist deposition, accretion, and cooling to within a time interval of ~10 m.y. (Grove et al., 2003).

We investigate the formation of inverted metamorphism in the Pelona Schist using a two-dimensional (2-D) thermokinematic model of flat subduction initiation and continuous schist

accretion. Metamorphic and thermochronologic data from the Sierra Pelona mountains and East Fork (San Gabriel River) exposures of the Pelona Schist (Fig. 1) are used to estimate, based on a formal inversion of the model parameters, the influence of shear heating on the formation of inverted metamorphism and the effects of uncertainty regarding input parameters.

GEOLOGIC BACKGROUND

Two major tectonic units comprise the San Gabriel Mountains (Fig. 1): Late Cretaceous upper plate calc-alkaline intrusions and their metamorphic framework, and lower plate Pelona Schist (Ehlig, 1981). The Pelona Schist is part of a group of Late Cretaceous, Franciscan-affinity trench and possibly forearc sediments structurally juxtaposed beneath plutonic rocks of slightly older age across southern California (Fig. 1A). The schists are contiguous at depth with a thickness of >10 km (Porter et al., 2011). Schist emplacement and flat subduction coincided with the subduction of a large igneous province (Liu et al., 2010; Saleeby, 2003). Plate convergence at the time was ~100 km/m.y. (e.g., Liu et al., 2010). Subduction was extremely shallow, juxtaposing schist against plutonic rocks ~300 km inboard of the trench at depths of ~30 km (Grove et al., 2003; Saleeby, 2003). The schists were metamorphosed at ~0.8–1 GPa (Chapman et al., 2011; Graham and Powell, 1984; Jacobson, 1995; Kidder and Ducea, 2006). In the few places where finite strains can be estimated, X/Z axial ratios are generally high (>8; Chapman et al., 2010). Isoclinally refolded folds are widespread (Jacobson, 1983).

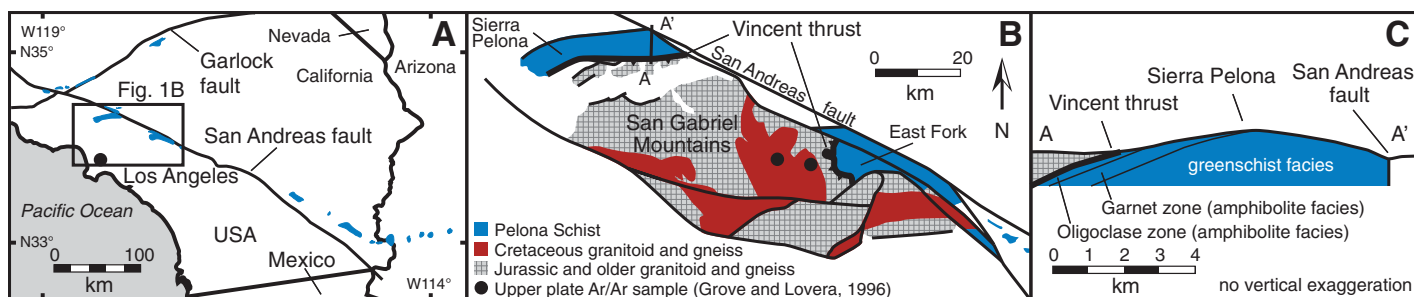


Figure 1. A: Map of southern California (United States) and vicinity showing Pelona Schist and related schists in blue. B: Map of San Gabriel Mountains (after Ehlig, 1981). C: Cross section of Sierra Pelona showing inverted metamorphic gradient (following Graham and England, 1976).

*Current address: Department of Geology, University of Otago, Dunedin 9054, New Zealand.

The schist was accreted either gradually (e.g., continuous accretion mechanism; Peacock, 1987) or episodically. We assume that accretion occurred at a constant rate based on the high strains and substantial thickness of the schist and the absence of observed major internal shear zones (Jacobson, 1995).

THERMOCHRONOLOGIC AND THERMOBAROMETRIC DATA

Exposed structural thicknesses of the Pelona Schist in the Sierra Pelona and East Fork are ~1 and ~4 km, respectively (Ehlig, 1981). In the Sierra Pelona, garnet-hornblende temperature estimates decrease from ~620 °C at uppermost levels of the schist to ~480 °C at a structural depth of 600–700 m (Fig. 2; Graham and Powell, 1984). Inverted metamorphism has not been detected in the (entirely) greenschist facies East Fork schist. Available thermobarometric data, Ar/Ar cooling ages (Grove and Lovera, 1996; Jacobson, 1990; Miller and Morton, 1980), and ages of youngest detrital zircons (Grove et al., 2003) are plotted versus structural depth in Figure 2.

FORWARD AND INVERSE MODEL DESCRIPTION

The forward model is a 2-D modification of the finite element program Pecube (Braun, 2003) with flat topography. The grid size is 250 m. Thermal diffusivity is assumed to be 25 km²/m.y. Radiogenic heat production is based on the geochemical analysis of Brady et al. (2006) in the southern Californian arc (Table 1). The model begins with separate geotherms for the continent and material to be subducted (forearc and oceanic crust). Subduction occurs on a fault with ramp-flat geometry. A thin layer along the top of the subducting slab is continuously added to the base of the upper plate in an accretion zone (Fig. 3). Tracers record the thermal histories of upper plate particles in the accretion zone and the schist as it is added to the upper plate. Accretion begins when the first particles subducted from the surface reach the accretion

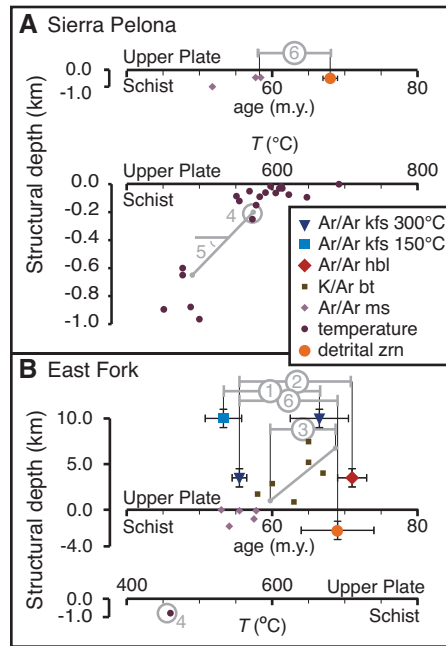


Figure 2. Thermochronologic (temperature, *T*) and metamorphic constraints (colored symbols; see text for sources) and results from best-fit models (gray) for two Pelona Schist localities. **A:** Sierra Pelona mountains. **B:** East Fork (San Gabriel River). Gray numbers label six constraints used to compare model results to geologic data: (1) time taken to cool from 300 to 150 °C at point 10 km above thrust; (2) time taken to cool from 500 to 300 °C at point 3.5 km above thrust; (3) time between cooling through ~300 °C 1 km and 7 km above schist; (4) peak metamorphic temperature in schist at depth of 200 m; (5) magnitude of inverted metamorphic gradient between depths of 200 and 650 m; (6) age difference between youngest detrital zircon in schist and Ar/Ar cooling age of upper plate or schist (see Table 2). Gray lines depict values of these constraints for best-fit models; e.g., in A, there is good match between model results (inclined gray line) and metamorphic data (dark purple). hbl—hornblende; ms—muscovite; kfs—potassium feldspar; bt—biotite; zrn—zircon. Numerical values and uncertainties for each criterion are given in Table 2.

zone. Shear heating throughout the medium is the product of the strain rate tensor and stress (e.g., Graham and England, 1976). The model is purely kinematic, with strain occurring only on fixed surfaces (Fig. 3) of thickness dictated by the grid spacing. A single uniform stress magnitude is assumed throughout the model, hence shear heating is a linear function of strain rate. Thermal boundary conditions and additional information on the model are given in the GSA Data Repository¹.

A neighborhood algorithm inversion (Sambridge, 1999) was used to find satisfactory models and determine ranges of input parameters permitted by constraints. Nine parameters varied independently: five geometric and kinematic variables depicted in Figure 3, the initial geotherms of continent and subducted crust, radiogenic heat production, and shear stress (τ). Allowed values for the nine parameters are within plausible ranges given geologic uncertainty (Table 1). (For further information

on the geotherms and heat production parameters, see the Data Repository.) Consistency with independent constraints was based on the least squares misfit function ψ ,

$$\psi = \frac{1}{N} \sum_{i=1}^N \frac{(x_{i,m} - x_{i,o})^2}{\sigma_i^2}, \quad (1)$$

where $x_{i,o}$ are the values of up to five metamorphic and thermobarometric constraints (Fig. 2), $x_{i,m}$ are the corresponding model results, and σ_i is the standard deviation (where available) or estimated error of the constraints (Table 2). Two inversions were run, one each for the two schist localities.

RESULTS

Figure 4 demonstrates how thermochronologic data and inverted metamorphism are reproduced by depicting the thermal evolution along particle paths predicted by a model with low misfit. (For examples of the 2-D thermal evolution of the model, see the Data Repository.)

TABLE 1. MODEL INPUT VARIABLES AND RANGES, AND OUTPUT VALUES FROM BEST-FIT MODELS

	Convergence rate (km/m.y.)	Trench-schist distance (km)	Accretion rate (km/m.y.)	Underplate width (km)	Subduction depth (km)	Ocean crust age* (m.y.)	Arc temp at 30 km [†] (°C)	Shear stress (MPa)	Heat production [§] (%)
Allowed	80–130	140–250 [#]	0.1–10	20–150	20–40	30–50	450–700	0–100	50–150
Sierra Pelona	118	179	1.1	102	35	39	696	3	78
East Fork	98	170	0.8	124	26	42	455	22	90
Figure 4 model	126	386	0.6	115	33	32	627	5	83

*Oceanic geotherm follows Turcotte and Schubert (2002).

[†]Continental geotherm is an oceanic geotherm (Turcotte and Schubert, 2002) passing through these values.

[§]Heat production varies 50% higher and lower than the profile estimated by Brady et al. (2006).

[#]Trench-schist distances up to 400 km were allowed in the Figure 4 model.

¹GSA Data Repository item 2013247, details of initial and boundary conditions, scatter plots comparing nine input parameters, and modeled thermal structure with time, is available online at www.geosociety.org/pubs/ft2013.htm, or on request from editing@geosociety.org or Documents Secretary, GSA, P.O. Box 9140, Boulder, CO 80301, USA.

Figure 3. Model geometry and kinematics. Dotted line separates initial geothermal gradients of continent and material to be subducted. Vertical uplift in accretion zone of width (w) is superimposed within flat subduction segment of depth (z) when sediment first arrives at distance (d) from trench. Accretion and surface erosion thereafter occur continuously at constant rate (u). Dark blue—accreted schist. Light blue shaded area—sediments that will become schist. Deformation (and accompanying shear heating) occurs only along thin deformation zones (gray) and plate boundary.

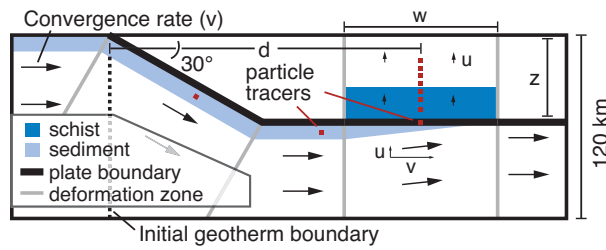


TABLE 2. MODEL CONSTRAINTS DEPICTED IN FIGURE 2

Pelona Schist occurrence	1. K-feldspar (m.y. \pm 1 σ)	2. Hornblende–K-feldspar (m.y. \pm 1 σ)	3. Δ Biotite age (m.y. \pm 1 σ)	4. Peak temperature ($^{\circ}$ C \pm 1 σ)	5. Inverted gradient ($^{\circ}$ C/km \pm 1 σ)	6. Zircon (m.y. \pm 1 σ)
Sierra Pelona	NA	NA	NA	587 \pm 50	180 \pm 25	10.0* \pm 2.0
East Fork	13.2 \pm 4.7	15.5 \pm 2.2	8.4 \pm 5.6	460 \pm 50	NA	13.5† \pm 5.1

*Minimum age difference between youngest detrital zircon (68 \pm 2 Ma) and Ar/Ar muscovite (58.2 \pm 1) at depth \sim 0.5 km in the schist.

†Minimum age difference between youngest detrital zircon at a depth of 3 km in the schist (69 \pm 5 Ma), and Ar/Ar K-feldspar 300 $^{\circ}$ C cooling age (55.5 \pm 1 Ma) 3.5 km above contact.

Figure 5 shows how misfit varies as a function of τ and accretion rate. Well-fitting models ($\psi < 2$) require an accretion rate of 0.1–3.6 km/m.y. and $\tau < 19$ and $\tau < 58$ MPa, respectively, for the Sierra Pelona and East Fork schists. The Sierra Pelona model requires a minimum initial décollement temperature of \sim 600 $^{\circ}$ C. The remaining six parameters are not well correlated with fit (see the Data Repository), indicating that the results are independent of assumptions about heat production, convergence rate, accretion zone geometry, and the thermal profile of the downgoing plate. Best-fit model parameters are given in Table 1. Results are compared to geologic constraints in Figure 2.

DISCUSSION

No shear heating is required to successfully model the inverted metamorphism and thermochronologic data (Fig. 5). The modeled inverted metamorphic gradients result from cooling during continuous accretion (type 2 inverted gradient of Peacock, 1987). Peak metamorphism of upper levels of the schist is generally reached during accretion (e.g., Fig. 4), thus the rate of cooling of the accretion zone divided by the accretion rate equals the recorded gradient. Shear heating actually inhibits the formation of the modeled gradients (Fig. 6) because it reduces the cooling rate. This relationship was not observed in earlier Pelona Schist models (England and Molnar, 1993; Graham and England, 1976; Peacock, 1987) because they did not incorporate accretion.

High τ of \sim 100 MPa (England and Molnar, 1993; Graham and England, 1976) is not only unnecessary to explain inverted metamorphism in the Sierra Pelona, but prohibited (in this

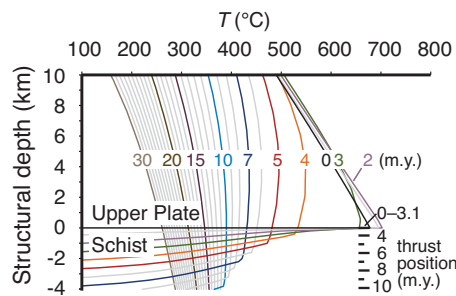


Figure 4. Thermal (temperature, T) evolution of model showing how inverted gradient is progressively produced during continuous accretion. Selected model shows good fit to both East Fork and Sierra Pelona (see text) constraints. Contours are based on thermal histories of 70 particles (some far traveled) that end up in center of accretion zone. Numbers indicate time (m.y.) since model initiation. Inverted gradient in upper 4 km of schist is assembled between 3.1 and 10 m.y. and does not coincide with thermal gradient that existed at any one time. The \sim 25 $^{\circ}$ C upper plate temperature increase between 0 and 2 m.y. is due to minor shear heating (shear stress, $\tau = \sim$ 5 MPa). Shear heating is superimposed on overall cooling pattern and reduces recorded inverted gradient (see Fig. 6).

kinematic family of models). Maximum allowed τ is 19 MPa in the Sierra Pelona inversion. As low τ is also required to reproduce inverted metamorphism and thermochronologic data in the Himalaya (Herman et al., 2010), we know of no remaining inverted metamorphic gradients associated with high rates of shear heating.

The model we hypothesize for schist emplacement is testable. At accretion rates \sim 1 km/m.y.,

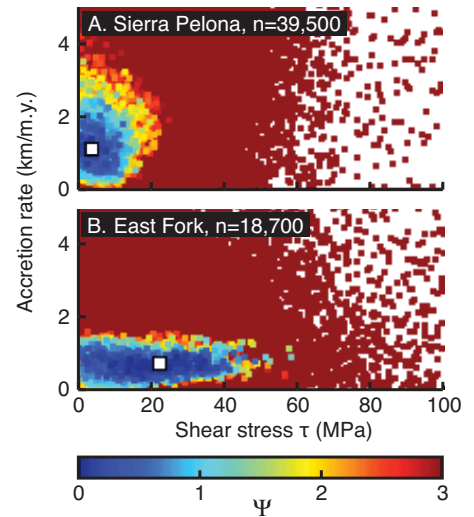


Figure 5. Results of neighborhood algorithm inversions for southern California localities. A: Sierra Pelona mountains. B: East Fork (San Gabriel River). Each dot corresponds to model run; color indicates least squares misfit ψ between observations and predictions. A ψ value of 1 is equivalent to 1 σ average misfit. Models are plotted in order of decreasing ψ such that better models overlay poorer models. Good models (blue) are limited to low τ and low accretion rates. Best-fit models are plotted as white squares. Models with accretion rates $>$ 5 km/m.y. are shown in the Data Repository figures (see footnote 1; all have high misfits).

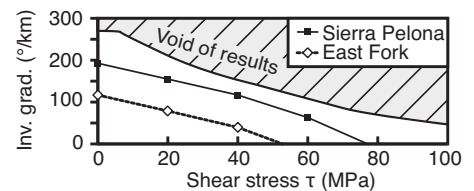


Figure 6. Inverted gradients (inv. grad.) as function of τ for the best-fit models (see Table 1). Gradients decrease with increasing τ (others are variables are held constant at values given in Table 1). High- τ noninverted gradients are not plotted. No models ($n = 227,000$) plot within labeled void.

detrital zircons should be \sim 4 m.y. younger at the bottom of the East Fork section than at the top. Alternatively, the models of Graham and England (1976) and England and Molnar (1993) allow for youngest zircons at the top of the schist. The results can also be tested against τ estimated in rock samples using recrystallized grain size piezometry, a tool that may be significantly more accurate than previously recognized (Kidder et al., 2012).

ACKNOWLEDGMENTS

We benefited from comments by J. Stock, J. Scott, and reviews by John Platt, Pavel Pitra, Marcel Frehner, and an anonymous reviewer. The Gordon and Betty Moore Foundation via Caltech's Tectonics

Observatory provided financial support. Computations were performed on the Pangu facility at Caltech. This is Caltech Tectonics Observatory contribution 226.

REFERENCES CITED

- Brady, R.J., Ducea, M.N., Kidder, S.B., and Saleeby, J.B., 2006, The distribution of radiogenic heat production as a function of depth in the Sierra Nevada Batholith, California: *Lithos*, v. 86, p. 229–244, doi:10.1016/j.lithos.2005.06.003.
- Braun, J., 2003, Pecube: A new finite-element code to solve the 3D heat transport equation including the effects of a time-varying, finite amplitude surface topography: *Computers & Geosciences*, v. 29, p. 787–794, doi:10.1016/S0098-3004(03)00052-9.
- Chapman, A.D., Kidder, S., Saleeby, J.B., and Ducea, M.N., 2010, Role of extrusion of the Rand and Sierra de Salinas schists in Late Cretaceous extension and rotation of the southern Sierra Nevada and vicinity: *Tectonics*, v. 29, doi:10.1029/2009TC002597.
- Chapman, A.D., Luffi, P.L., Saleeby, J.B., and Petersen, S., 2011, Metamorphic evolution, partial melting and rapid exhumation above an ancient flat slab: Insights from the San Emigdio Schist, southern California: *Journal of Metamorphic Geology*, v. 29, p. 601–626, doi:10.1111/j.1525-1314.2011.00932.x.
- Cooper, A.F., and Norris, R.J., 2011, Inverted metamorphic sequences in Alpine fault mylonites produced by oblique shear within a plate boundary fault zone, New Zealand: *Geology*, v. 39, p. 1023–1026, doi:10.1130/G32273.1.
- Ehlig, P.L., 1981, Origin and tectonic history of the basement terrane of the San Gabriel Mountains, Central Transverse Ranges, in Ernst, W.G., ed., *The geotectonic development of California* (Rubey Volume 1): Englewood Cliffs, New Jersey, Prentice-Hall, p. 253–283.
- England, P.C., and Molnar, P., 1993, The interpretation of inverted metamorphic isograds using simple physical calculations: *Tectonics*, v. 12, p. 145–157, doi:10.1029/92TC00850.
- Graham, C.M., and England, P.C., 1976, Thermal regimes and regional metamorphism in the vicinity of overthrust faults: An example of shear heating and inverted metamorphic zonation from southern California: *Earth and Planetary Science Letters*, v. 31, p. 142–152, doi:10.1016/0012-821X(76)90105-9.
- Graham, C.M., and Powell, R., 1984, A garnet-hornblende geothermometer: Calibration, testing, and application to the Pelona Schist, southern California: *Journal of Metamorphic Geology*, v. 2, p. 13–31, doi:10.1111/j.1525-1314.1984.tb00282.x.
- Grove, M., and Lovera, O.M., 1996, Slip history of the Vincent thrust: Role of denudation during shallow subduction, in *Bebout, G.E., et al., eds., Subduction top to bottom: American Geophysical Union Geophysical Monograph 96*, p. 163–170, doi:10.1029/GM096p0163.
- Grove, M., Jacobson, C.E., Barth, A.P., and Vucic, A., 2003, Temporal and spatial trends of Late Cretaceous–early Tertiary underplating of Pelona and related schist beneath southern California and southwestern Arizona, in *Johnson, S.E., et al., eds., Tectonic evolution of northwestern Mexico and the southwestern USA: Geological Society of America Special Paper 374*, p. 381–406, doi:10.1130/0-8137-2374-4.381.
- Harrison, T.M., Grove, M., Lovera, O.M., Catlos, E.J., and D’Andrea, J., 1999, The origin of Himalayan anatexis and inverted metamorphism: Models and constraints: *Journal of Asian Earth Sciences*, v. 17, p. 755–772, doi:10.1016/S1367-9120(99)00018-8.
- Herman, F., Copeland, P., Avouac, J.-P., Bollinger, L., Mahéo, G., Fort, P.L., Rai, S., Foster, D., Pêcher, A., Stüwe, K., and Henry, P., 2010, Exhumation, crustal deformation, and thermal structure of the Nepal Himalaya derived from the inversion of thermochronological and thermobarometric data and modeling of the topography: *Journal of Geophysical Research*, v. 115, B06407, doi:10.1029/2008JB006126.
- Jacobson, C.E., 1983, Structural geology of the Pelona Schist and Vincent thrust, San Gabriel Mountains, California: *Geological Society of America Bulletin*, v. 94, p. 753–767, doi:10.1130/0016-7606(1983)94<753:SGOTPS>2.0.CO;2.
- Jacobson, C.E., 1990, The $^{40}\text{Ar}/^{39}\text{Ar}$ geochronology of the Pelona Schist and related rocks, southern California: *Journal of Geophysical Research*, v. 95, p. 509–528, doi:10.1029/JB095iB01p00509.
- Jacobson, C.E., 1995, Qualitative thermobarometry of inverted metamorphism in the Pelona and Rand Schists, southern California, using calciferous amphibole in mafic schist: *Journal of Metamorphic Geology*, v. 13, p. 79–92, doi:10.1111/j.1525-1314.1995.tb00206.x.
- Jamieson, R.A., Beaumont, C., Hamilton, J., and Fullsack, P., 1996, Tectonic assembly of inverted metamorphic sequences: *Geology*, v. 24, p. 839–842, doi:10.1130/0091-7613(1996)024<0839:TAOIMS>2.3.CO;2.
- Kidder, S., and Ducea, M., 2006, High temperatures and inverted metamorphism in the schist of Sierra de Salinas, California: *Earth and Planetary Science Letters*, v. 241, p. 422–437, doi:10.1016/j.epsl.2005.11.037.
- Kidder, S., Avouac, J.P., and Chan, Y.C., 2012, Constraints from rocks in the Taiwan orogen on crustal stress levels and rheology: *Journal of Geophysical Research*, v. 117, B09408, doi:10.1029/2012JB009303.
- Le Fort, P., 1975, Himalayas: The collided range. Present knowledge of the continental arc: *American Journal of Science*, v. 275-A, p. 1–44.
- Liu, L., Gurnis, M., Seton, M., Saleeby, J., Müller, R.D., and Jackson, J.M., 2010, The role of oceanic plateau subduction in the Laramide orogeny: *Nature Geoscience*, v. 3, p. 353–357, doi:10.1038/ngeo829.
- Miller, F.K., and Morton, D.M., 1980, Potassium-argon geochronology of the eastern Transverse Ranges and southern Mojave Desert, southern California: *U.S. Geological Survey Professional Paper 1152*, 30 p.
- Nabelek, P.I., Whittington, A.G., and Hofmeister, A.M., 2010, Strain heating as a mechanism for partial melting and ultrahigh temperature metamorphism in convergent orogens: Implications of temperature-dependent thermal diffusivity and rheology: *Journal of Geophysical Research*, v. 115, B12417, doi:10.1029/2010JB007727.
- Peacock, S.M., 1987, Creation and preservation of subduction-related inverted metamorphic gradients: *Journal of Geophysical Research*, v. 92, p. 12763–12781, doi:10.1029/JB092iB12p12763.
- Pitra, P., Ballèvre, M., and Ruffet, G., 2010, Inverted metamorphic field gradient towards a Variscan suture zone (Champtoceaux Complex, Armorican Massif, France): *Journal of Metamorphic Geology*, v. 28, p. 183–208, doi:10.1111/j.1525-1314.2009.00862.x.
- Porter, R., Zandt, G., and McQuarrie, N., 2011, Pervasive lower-crustal seismic anisotropy in southern California: Evidence for underplated schists and active tectonics: *Lithosphere*, v. 3, p. 201–220, doi:10.1130/L126.1.
- Saleeby, J.B., 2003, Segmentation of the Laramide slab—Evidence from the southern Sierra Nevada region: *Geological Society of America Bulletin*, v. 115, p. 655–668, doi:10.1130/0016-7606(2003)115<0655:SOTLSF>2.0.CO;2.
- Sambridge, M., 1999, Geophysical inversion with a neighbourhood algorithm—I. Searching a parameter space: *Geophysical Journal International*, v. 138, p. 479–494, doi:10.1046/j.1365-246X.1999.00876.x.
- Turcotte, D.L., and Schubert, G., 2002, *Geodynamics*: Cambridge, UK, Cambridge University Press, 456 p.

Manuscript received 6 December 2012

Revised manuscript received 2 April 2013

Manuscript accepted 3 April 2013

Printed in USA